ScientificScholar®
Knowledge is power
Publisher of Scientific Journals

https://arabjchem.org

Arabian Journal of Chemistry

Article in Press

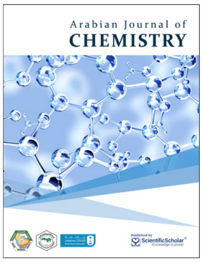

Original Article

Soft-template synthesis of carbon-doped mesoporous TiO_2 using *Citrullus colocynthis* fruit shell extract: Characterization and photocatalytic application

Mohammed H. Geesi*

Department of Chemistry, College of Science and humanities in Al-Kharaj, Prince Sattam bin Abdulaziz Univesity, Al-Kharaj 11942, Saudi Arabia.

ARTICLE INFO

Keywords:
Citrullus colocynthis
Dye degradation
Intrinsic C-doped TiO_2
Soft-template sol-gel synthesis

ABSTRACT

Mesoporous structured Titanium dioxide (TiO_2) inherently carbon-doped was synthesized by a soft-templating sol-gel approach using *Citrullus colocynthis* fruit shell aqueous extract. Several techniques, including X-ray diffraction (XRD), scanning electron microscope (SEM), transmission electron microscopy (TEM), X-ray photoelectron spectroscopy (XPS), ultraviolet (UV)-visible spectroscopy, and Fourier transform infra-red spectroscopy (FTIR), were used to determine the structural and electronic features of the synthesized TiO_2. Together, XRD and High-resolution transmission electron microscopy (HRTEM) analysis confirmed the formation of a polycrystalline anatase TiO_2 polymorph with edge dislocation. XPS analysis confirmed the effective creation of carbon self-doped TiO_2 with induced oxygen vacancies. The photodegradation potential of the synthesized TiO_2 was assessed on methylene blue by UV irradiation. A 71.5% degradation rate was observed in 150 mins of exposure to UV radiation.

1. Introduction

Titanium dioxide (TiO_2), notably its anatase polymorph, is a photoactive semiconductor extensively applied as an ecofriendly catalyst for the degradation of versatile organic pollutants originating from the overuse of items like dyes and pharmaceuticals after their discharge into aquatic mediums [1,2]. The degradation mechanism of these pollutants relies on the photogeneration of electron-hole pairs under light excitation [3,4]. Electron-hole pairs diffuse to the TiO_2 surface to react with pollutants and degrade them. However, the anatase TiO_2 bandgap, reported to be about 3.2 eV, is large enough, restricting its photoactivation to only under the Ultraviolet light (UV) range [5]. Furthermore, despite relatively better photoactivity under UV light as compared to other TiO_2 polymorphs (rutile and brookite), rapid recombination of the generated electron-hole pairs in anatase represents a further hurdle. Therefore, pristine anatase TiO_2 remains an unsatisfactory photocatalyst.

In this way, the defect-engineering approach, notably surface defects, consists of the generation of tuned desired defects to boost the photocatalytic performance of TiO_2 by altering its structural, morphological, and electronic features as well as the modulation of the charge carriers concentration and separation. It is a widely applied approach [6,7]. Defects act as trap centers for photogenerated charge carriers, enhancing their separation efficiency and narrowing the bandgap. Several methods have been used to generate surface defects in TiO_2 and can be categorized as ex-situ if used post the synthesis process, including ion spurting, UV irradiation, plasma treatment, etc., and in-situ if used during the synthesis process, including doping, synthesis route, and annealing temperature and environment [8]. Unfortunately, these methods impact not only the surface properties of the synthesized nanostructures but also their shape, size, porosity, and crystallinity, which deny the advantages of the generated defects.

Alternatively, the soft-template synthesis approach has witnessed growing interest due to its ability to tune both the morphological and physicochemical features of the derived TiO_2 nanostructures [9]. Generally, organic-based materials, such as surfactants, block polymers, or flexible organic molecules, are commonly introduced in the synthesis medium as soft templates that act as scaffolds to guide the growth of the nanostructures [9,10]. In this process, positive metal ions of the precursor self-assemble to specific sites of the soft template via electrostatic interactions. The template can be removed at the end of the reaction using different physicochemical approaches, such as dissolution or calcination.

Additionally, plants, as biological templates, have been acknowledged for their ability to produce versatile highly ordered metal and metal oxide nanostructures associated with the abundance of versatile biomolecules in their composition, such as polyphenols, tannins, terpenoids, proteins, flavonoids, alkaloids, limonoids, amino acids, etc., which act as intrinsic reducing, capping, complexing, and structure-directing agents [11,12]. Thus, functional groups (carboxylic, hydroxyl, amine, etc.) of plant biomolecules bind to metal ions via electrostatic forces, while the carbon skeletons act as nucleation sites for the metal ions. After calcination, the organic template decomposes together with the leakage of CO_2 and H_2O, leading to the formation of porous nanostructures. Advantageously, these porous nanostructures are achieved without the need for any additional surface modifying or templating agents commonly used in chemical-based soft-template methods [13,14].

Citrullus colocynthis, also known as bitter apple, is a medicinal plant endemic to several dry regions of Asia and Africa, including Saudi

---

***Corresponding author:**
E-mail address: m.geesi@psau.edu.sa (M. Geesi)

Received: 02 December, 2024 **Accepted:** 06 February, 2025 **Epub Ahead of Print:** 31 March 2025 **Published:** ***
DOI: 10.25259/AJC_214_2024

Arabia. Its seeds and fruits are particularly rich in phytoelements, such as glycosides, flavonoids, phenolics, and fatty acids, giving it versatile medicinal applications due to anti-hyperglycemic [15], anti-fungal [16], and anti-obesity [17] attributes.

Earlier, magnesium oxide nanosheets were prepared using the fruit extract of *Citrullus colocynthis* and used as catalysts for biofuel production [18]. Recently, gold nanoparticles were synthesized using the *Citrullus colocynthis* pulp fruit extract and assessed for different biological activities [19]. So far, no one has used *Citrullus colocynthis* extracts for the synthesis of TiO_2.

Herein, mesostructured TiO_2 was synthesized using a soft-templating sol-gel approach profiting from the abundance of various phytoelements in the *Citrullus colocynthis* fruit shell aqueous extract with dual reducing and structure-directing effects. Interestingly, besides the abovementioned benefits, the extract offers an intrinsic carbon doping of the synthesized TiO_2. Overall, this study provides a simple, easy, and cost-effective approach for the synthesis of mesoporous TiO_2, taking advantage of the abundance of various biomass template materials.

2. Materials and Methods

2.1. Preparation of TiO_2

Wild *Citrullus colocynthis* fruits were collected from the Jizan province of Saudi Arabia. The fruits were dried at room temperature and the shells were harvested and ground. 4 g of the obtained powder was added to 100 mL of deionized water and heated at 60°C for 30 mins. The harvested extract will be used as a stock solution for synthesizing TiO_2 samples. The preparation of the TiO_2 nanoparticles was achieved by sol-gel route, as described previously [20,21]. Specifically, 17 mL of Tetra (2-ethylhexyl) titanate (from Sigma Aldrich) was mixed with 17 mL of ethanol and stirred for 30 mins, then 17 mL of the extract stock solution was added to the precursor/ethanol solution while stirring for 30 mins, as a result of which the mixture transformed rapidly to gel. The gel was kept to dry overnight in pre-heated oven at 80°C. The dried powder was ground in a mortar, poured into a ceramic crucible, and annealed at 600°C for 2 hrs.

2.2. Characterization techniques

The crystal structure of the as-synthesized TiO_2 was revealed by a Rigaku Ultima IV diffractometer acquired from Bruker and equipped with Cu-Kα source providing wavelength $\lambda = 0.15406$ nm. Diffraction data were performed in the 2θ angle range 10-80° with a step of 0.02°. UV–Vis-NIR spectrophotometer from Agilent Company was used to perform the optical absorption spectra. Infrared spectroscopy investigations were conducted by a Thermo Scientific Nicolet iS50 spectrometer. An Inspect F50 scanning electron microscope (SEM) from FEI Company was used for the morphological studies of the synthesized TiO_2 samples. Thermogravimetric experiment (TGA) was performed by a TGA Shimadzu DTG-60. Photocatalytic degradation experiments of methylene blue (MB) were conducted in a photocatalytic reactor equipped with a 300-W xenon UV lamp (CEL-PF300-16, Beijing China Education AuLight Technology Co., LTD., Beijing, China) providing an intensity of ~125 mW/cm².

2.3. Catalytic activity

The photocatalytic activity of synthesized TiO_2 towards the decomposition of methylene blue (from Sigma Aldrich) under UV excitation was evaluated on a UV-visible spectrophotometer. 10 mg of MB dye was dissolved in 1L of deionized water to form a dye stock solution. Next, 200 mL of the stock solution was mixed with 5 mg of the synthesized TiO_2 under vigorous stirring. Afterwards, the solution was illumined by a UV source, and every 15 mins, 2 mL were taken and subjected to a UV absorbance experiment. The methylene blue removal efficiency was calculated by the following formula (Eq. 1):

$$\%D = \frac{A_0 - A_t}{A_0} \times 100 \qquad (1)$$

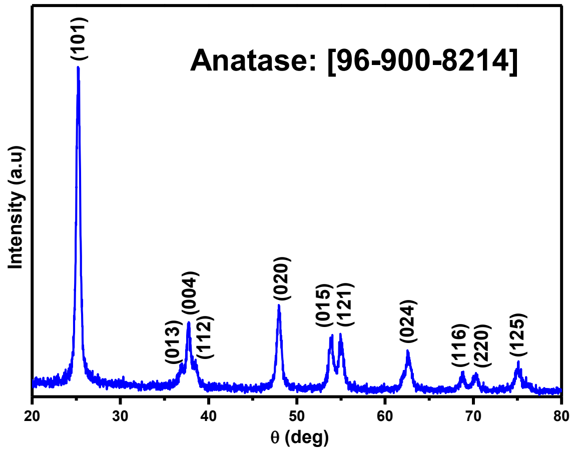

Figure 1. XRD diffraction pattern of the synthesized TiO_2.

Where, A_0 and A_t represent the initial maxima of the absorbance of the methylene blue solution and that of the solution after being irradiated under UV during a given time interval t.

3. Results and Discussion

3.1. Crystallographic analysis

XRD explored the crystallographic structure of the as-synthesized TiO_2. As shown in Figure 1, diffraction peaks can be identified at 25.3°, 36.95°, 37.79°, 38.57°, 48.05°, 53.88°, 55.07°, 62.69°, 68.75°, 70.3°, and 75.05°, attributed to the crystallographic diffraction planes (101), (013), (004), (112), (020), (015), (121), (024), (116), (220), and (125), respectively. All these diffraction peaks are assigned to the anatase TiO_2 polymorph (JCPDS card no. 96-900-8214). The absence of any unidentified diffraction peaks in this pattern confirmed the high purity and crystallinity of the synthesized sample. Moreover, a thermodynamically stable anatase phase was achieved despite the fact that the synthesized TiO_2 was calcined at 600°C for two hrs. It is likely that the reason for such thermal stability is the complex composition of the *Citrullus colocynthis* extract, including versatile phytoelements and biomolecules that not only have reducing and capping effects beneficial for the growth of the TiO_2 nanoparticles but also promote the inhibition of anatase-to-rutile phase transition via carbon self-doping. Although the X-ray diffraction (XRD) pattern does not display any peaks revealing the existence of doping impurities in the TiO_2 structure, its thermal stability could be associated with the doping of lattice by carbon native to the plant extract as will be confirmed below by X-ray photoelectron spectroscopy (XPS) analysis. In fact, many authors suggested that anatase–to-rutile transformation can delayed by carbon doping [22,23].

The crystallite size of the synthesized TiO_2 was estimated by application of the Debye-Scherrer equation to the more intense diffraction peak located at 25.52° and assigned to the hkl crystallographic plane (101) [23]. The calculated mean size of crystallites was about 17.87 nm.

3.2. Thermal analysis

Thermogravimetric analysis (TGA) of the biosynthesized TiO_2 nanoparticles was performed at a heating rate of 10°C/min. The recorded TGA curve reveals a gradual reduction in mass that can be divided into three regions (Figure 2). The first, for temperatures below 200°C associated with the release of physisorbed water generated a mass loss of 5.9%. The second region between 200°C and 450°C, with a mass loss 8.9%, was likely attributed to the degradation of the organic compounds originating from the *Citrullus colocynthis* extract. After 450°C, the TGA curve consisted of a plateau, indicating the thermal stability of the synthesized TiO_2 beyond that temperature.

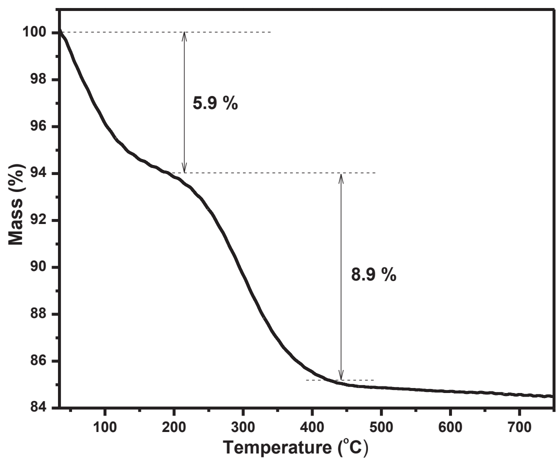

Figure 2. Thermogravimetric Analysis (TGA) curve of the synthesized TiO_2.

3.3. Morphologic analysis

Field emission scanning electron microscopy (FESEM) images of Figure 3(a) and 3(b) indicate that the synthesized TiO_2 exhibited an agglomerated morphology formed by spherical-shaped nanoparticles having an average diameter of 18 nm. The image also exhibits the presence of pores presumably associated with the removal of biomolecules included in the plant extract during the calcination process.

Furthermore, transmission electron microscopy (TEM) (Figure 3c and 3d) and high-resolution transmission electron microscopy (HRTEM) Figure 3(e) experiments were conducted to delve deeper into the structure and morphology of the synthesized TiO_2. The lattice arrangement of the synthesized TiO_2 with distinct grains and grain boundaries (marked with dashed lines) was observed, which revealed its polycrystalline nature. The high-resolution TEM image presented in Figure 3(e) exhibits the lattice fringes of the TiO_2 nanoparticles. Specifically, the interplanar lattice spacing of 0.352 nm refers to the typical (101) crystallographic plane of anatase polymorph in agreement

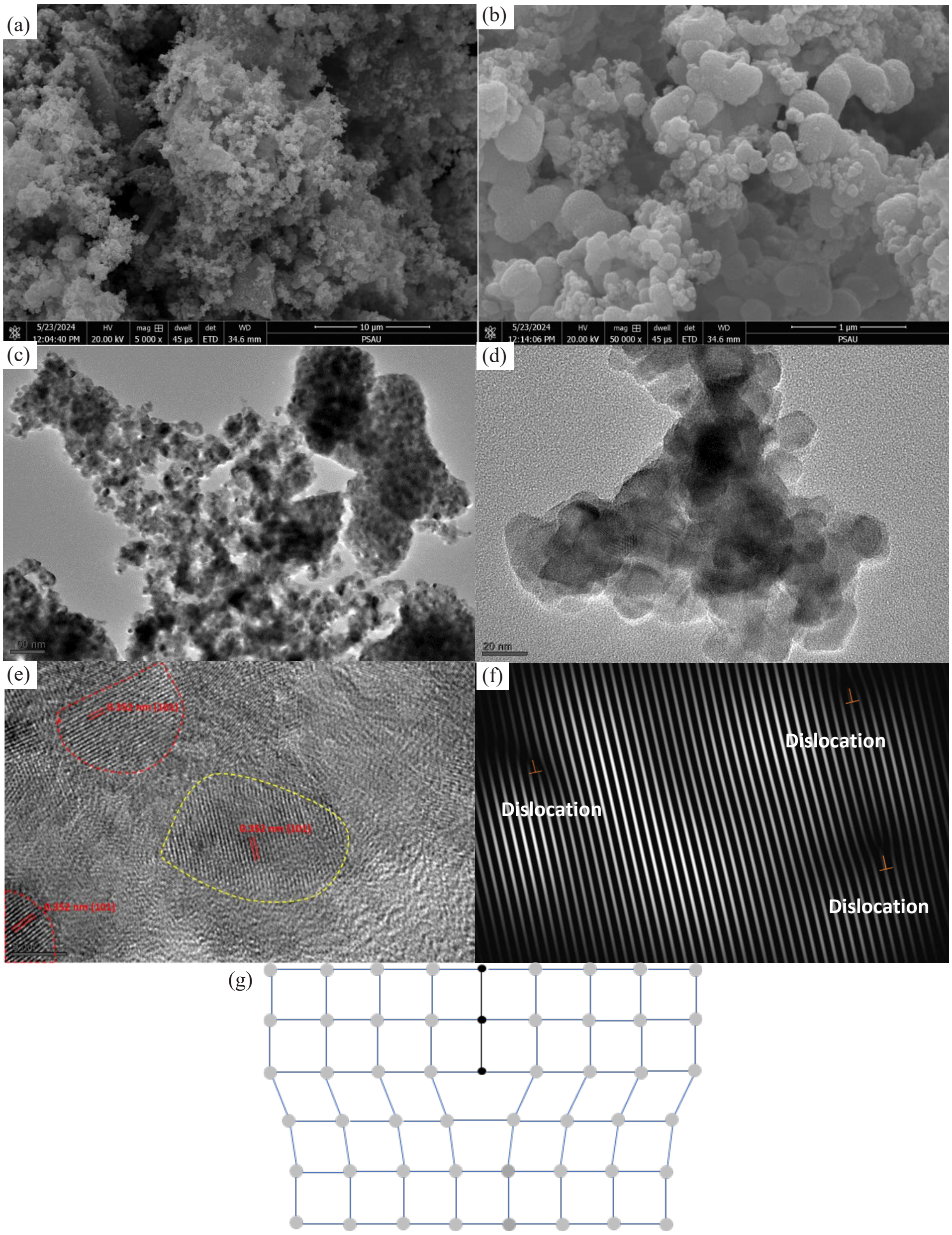

Figure 3. (a) and (b) SEM micrographs captured at two magnifications (x5000, x50000), (c) and (d) TEM images, (e) HRTEM of the synthesised TiO_2, (f) Inverse fast Fourier Transform (IFFT) of the yellow dashed delimited grain and (g) the schematic diagram of an edge dislocation. SEM: Scanning electron microscopy, TEM: Transmission electron microscopy, HRTEM: High-resolution transmission electron microscopy, IFFT: Inverse fast fourier transform.

with the XRD findings. In addition, the sample crystal lattice exhibits a certain stacking fault evidenced in inverse Fast Fourier transform (IFFT) performed on the yellow-dashed delimited region of (Figure 3e) and can be associated with edge dislocations (Figure 3f). Edge dislocation is a crystallographic defect that appears whenever an extra half-plane of atoms is introduced into the crystal lattice, triggering the distortion of nearby planes (Figure 3g). They are typically activated by the insertion of point defects in the crystal lattice, such as vacancies and heteroatoms, thereby acting as trap sites for the photogenerated charge carriers, which, in turn, improve photoactivity efficiency [24,25].

3.4. Infrared spectroscopy analysis

As can be seen in Figure 4, the FTIR spectrum of the synthesized TiO_2 exhibits a prominent band near 643 cm^{-1} ascribed to the Ti-O stretching vibration, confirming the formation of TiO_2 [26]. The absence of vibration bands specific to any organic groups confirmed the effective removal of the organic phase after the calcination step and indicated the purity of the synthesized TiO_2.

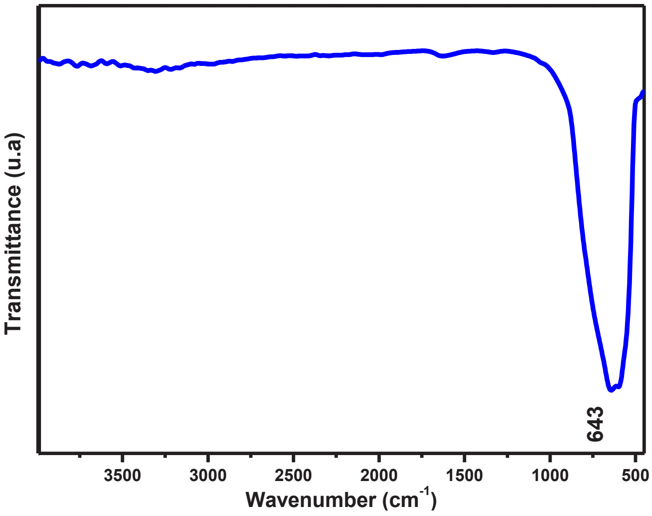

Figure 4. FTIR spectrum of the synthesised TiO_2.

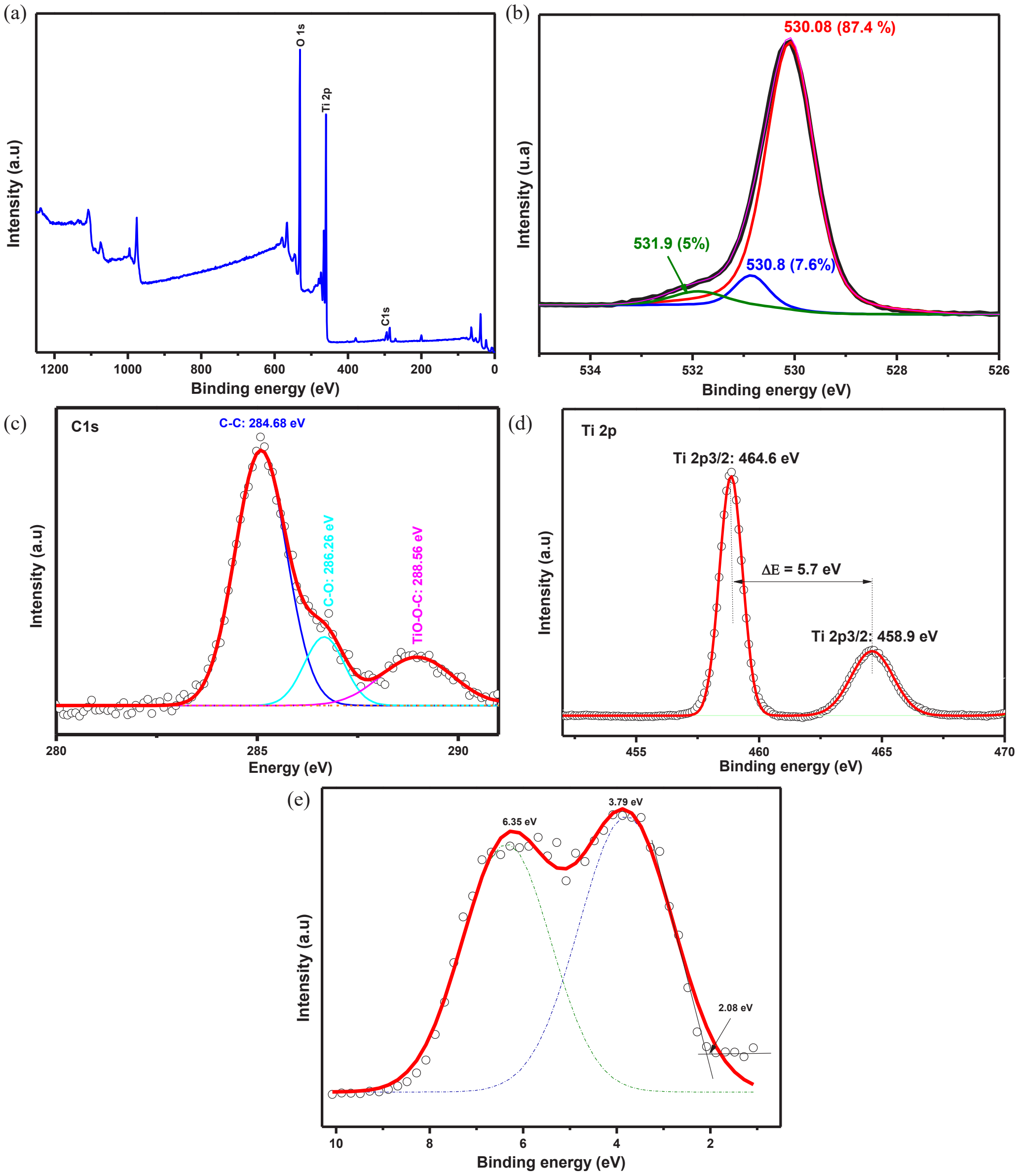

Figure 5. (a) XPS survey of the synthesised TiO2, high-resolution spectra of: (b) O1s, (c) C1s, (d) Ti2p and (e) valence energy. XPS: X-ray photoelectron spectroscopy, O1s: Oxygen 1s, C1s: Carbon 1s, Ti2p: Titanium 2p.

3.5. Elemental analysis

The surface chemical composition of the prepared TiO_2 was probed by X-ray photoelectron spectroscopy. The survey curve points out the presence of O, Ti, and C (Figure 5a). Further insightful investigations of the as-synthesized TiO_2 were achieved by recording the high-resolution peak spectra of the various elements revealed in the survey spectrum to check whether the growth approach generates any point defects such oxygen vacancy and doping in the synthesized TiO_2 structure (Figure 5b-d).

The asymmetric O 1s peak is fitted with three sub-peaks centered at 530.08 eV, 530.8 eV, and 531.9 eV and ascribed to the lattice oxygen, the oxygen vacancy, and the adsorbed oxygen, respectively, in agreement with several previous reports [27,28].

C1s spectrum was fitted into three peaks, where those situated at 284.68 eV, 286.26 eV, and 288.56 eV reflected that carbon exists in three different chemical environments. Indeed, the peak at 284.68 eV is attributed to the residual carbon element, whereas peaks at 286.26 eV and 288.56 eV are attributed to C=O and Ti-O-C, respectively [29]. The existence of a Ti–O–C bond associated with the oxygen substitution by carbon, together with the absence of any peaks around 282 eV characteristic of the Ti-C bond support that the carbon doping of the synthesized TiO_2 is either insertional or substitutional to O [30]. Previous experimental and theoretical studies suggest that such kind of doping induced many localized mid-bandgap states, improving the photoactivity potential of the synthesized TiO_2 by promoting the electron-hole separation [31].

The Ti2p high-resolution spectrum resolved in two peaks centered at 458 eV and 464 eV and assigned to the $Ti2p_{3/2}$ and $Ti2p_{1/2}$ spin-orbit splitting, respectively, indicating the presence of Ti^{4+} [32].

The valence band energy spectrum of the synthesized TiO_2 shown in Figure 5(e) was fitted by two Gaussian peaks centered at 3.73 eV and 6.25 eV, associated with the electron emission from π (nonbonding) and σ (bonding) O2p orbitals, respectively. These values correlated well with previous results on anatase TiO_2 [33,34]. Moreover, the valence band maximum (VBM) was determined by linear extrapolation of the valence band to the baseline to be 2.08 eV being barely equal to that previously reported for intrinsic carbon-doped TiO_2 prepared by solvothermal method (2.05 eV) [35].

3.6. UV-visible absorption

The optical absorption spectrum of the synthesized TiO_2 was conducted by scanning the wavelength range 200 nm - 800 nm, and the recorded data have been shown in Figure 6. The inset of Figure 6 represents the Tauc plot [36].

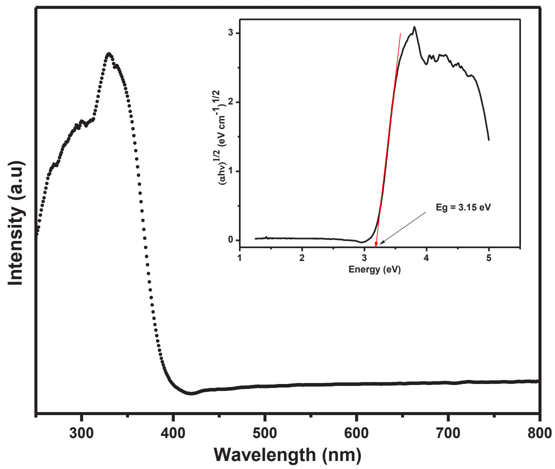

Figure 6. UV-visible absorption of the synthesised TiO_2, the inset represents the Tauc plot.

The optical bandgap of the as-synthesized TiO_2 derived from the Tauc plot was about 3.15 eV, nearly equal to the reported value for pristine anatase polymorph (3.2 eV) in line with previous studies stating that carbon-doping does not alter the band gap energy of TiO_2 significantly but promotes the separation of the electron-hole pairs [35,37].

3.7. Dye degradation

Photocatalysis is a process widely used for the degradation of dyes. This process mainly involves the use of heterogeneous catalysts, such as metal oxides and metal sulphides, metal–organic frameworks (MOFs), and appropriate light irradiation [38-40].

The photocatalytic potential of the as-synthesized TiO_2 nanostructures towards the degradation of methylene blue dye was evaluated via UV-visible absorption measurements. Figure 7(a) highlights a gradual decay of the absorption of methylene blue solution with UV irradiation time, reflecting the effectiveness of the synthesized TiO_2 in speeding up the degradation of MB. The maximum optical absorption of MB was achieved at a wavelength of 661.5 nm. A degradation rate of 71.5% was achieved

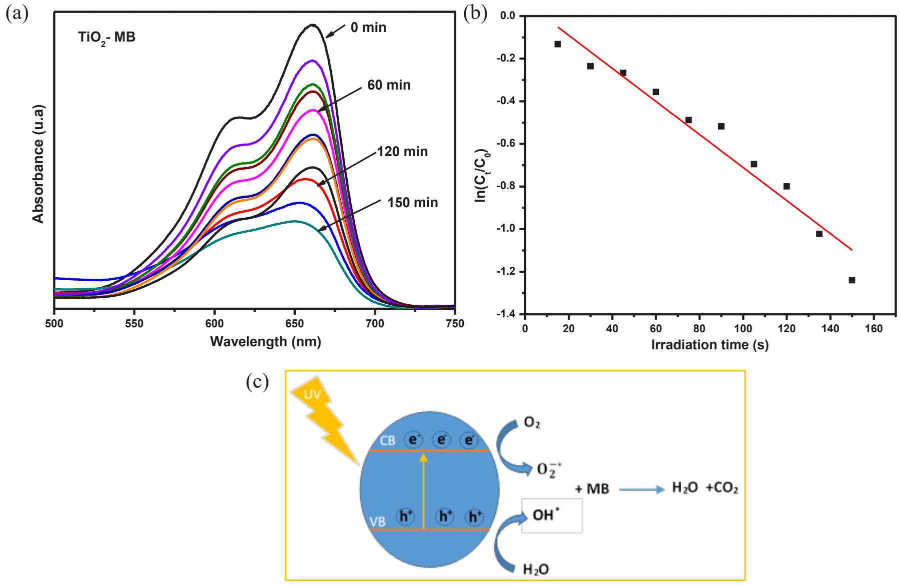

Figure 7. (a) Degradation of methylene blue by the synthesized TiO_2 under UV excitation, (b) Photocatalytic reaction's kinetics study by plotting $\ln\left(\frac{C_t}{C_0}\right)$ against irradiation time for the first order reaction degradation, (c) Plausible degradation mechanism. UV: Ultraviolet, CB: Conduction band, VB: Valence band, MB: Methylene blue, TiO_2: Titanium dioxide.

after 150 mins of UV irradiation. This compared well with a recent study carried out using cellulose nanocrystals (CNCs) as a template to synthesize TiO_2, achieving an MB degradation rate ranging from 65.3% to 79.9% according to the used mass concentration of CNCs [41].

To find out the photocatalytic reaction's kinetics model, $\ln\left(\frac{C_t}{C_0}\right)$ was plotted versus the irradiation time (Figure 7b). The obtained curve is fairly linear ($R^2 = 0.95$) with a slope k and can be described by the following Eq. (2):

$$\ln\left(\frac{C_t}{C_0}\right) = ln\left(\frac{A_t}{A_0}\right) = -kt \tag{2}$$

Where A_0 and A_t represent the absorption intensity at the maximum absorption wavelength (661.5 nm) for the MB solution without TiO_2 at (t=0) and that after being UV-irradiated in the presence of TiO_2 for a time interval t, respectively. The constant k that represents the reaction rate constant was found to be -0.0775 min^{-1}. The good linearity of the curve suggests that the degradation process follows a pseudo-first-order reaction's kinetics.

Conceptually, when TiO_2 is irradiated by a UV source, electrons jump from the valence band to the conduction band, leaving behind holes in the valence band. Therefore hole-electron pairs are created. Excited electrons in the conduction band react with molecular oxygen in air to produce superoxide anions, while holes in the valence band react with water molecules adsorbed on the photocatalyst surface to form hydroxyl radicals. The produced OH^* and O_2^{-*} radicals are highly reactive and can oxidize organic compounds near the surface of the photocatalyst. This oxidation process breaks down complex organic molecules into simpler substances, primarily CO_2 and H_2O. The presence of mid-gap sub-states acts as trapping sites for the charge carriers, which slows down their recombination to be more reactive to the environing species. The plausible degradation pathway of MB has been shown in Figure 7(c).

4. Conclusions

In this study, mesoporous TiO_2 was successfully synthesized by the sol-gel route using the *Citrullus colocynthis* fruit shell extract as a soft template. The synthesized TiO_2 was inherently doped with carbon accompanied by the occurrence of oxygen vacancies. Structurally, the C-doping introduced an edge dislocation, revealed using TEM analysis. With no significant change in bandgap energy of the synthesized TiO_2 (about 3.15 eV), these defects seemed to delay the charge carriers' recombination via the generation of mid-gap sub-states, which explains the enhancement of the photoactivity under UV irradiation. The photocatalytic ability of the synthesized TiO_2 towards the decomposition of methylene blue under UV irradiation was achieved with a rate of degradation of 71.5% attained after 150 mins of UV irradiation. The process of MB dye degradation model was found to follow a pseudo-first-order kinetics.

CRediT authorship contribution statement

Mohamed H. Geesi: Conceptualization; Data curation; Formal analysis; Funding acquisition; Investigation; Methodology; Project administration; Resources; Software; Supervision; Validation; Visualization; Writing – original draft; Writing – review & editing.

Declaration of competing interest

The author declare that they have no known competing financial interests or personal relationships that could have appeared to influence the work reported in this paper.

Declaration of Generative AI and AI-assisted technologies in the writing process

The authors confirm that there was no use of artificial intelligence (AI)-assisted technology for assisting in the writing or editing of the manuscript and no images were manipulated using AI.

Acknowledgement

This study is supported via funding from Prince sattam bin Abdulaziz University project number (PSAU/2025/R/1446).

References

1. Dong, H., Zeng, G., Tang, L., Fan, C., Zhang, C., He, X., He, Y., 2015. An overview on limitations of tiO2-based particles for photocatalytic degradation of organic pollutants and the corresponding countermeasures. *Water Research*, **79**, 128-146. https://doi.org/10.1016/j.watres.2015.04.038
2. Chen, D., Cheng, Y., Zhou, N., Chen, P., Wang, Y., Li, K., Huo, S., Cheng, P., Peng, P., Zhang, R., Wang, L., Liu, H., Liu, Y., Ruan, R., 2020. Photocatalytic degradation of organic pollutants using tiO2-based photocatalysts: A review. *Journal of Cleaner Production*, **268**, 121725. https://doi.org/10.1016/j.jclepro.2020.121725
3. Xu, H., Hao, Z., Feng, W., Wang, T., Li, Y., 2021. Mechanism of photodegradation of organic pollutants in seawater by tiO2-based photocatalysts and improvement in their performance. *ACS Omega*, **6**, 30698-30707. https://doi.org/10.1021/acsomega.1c04604
4. Ajmal, A., Majeed, I., Malik, R.N., Idriss, H., Nadeem, M.A., 2014. Principles and mechanisms of photocatalytic dye degradation on TiO 2 based photocatalysts: A comparative overview. *Rsc Advances*, **4**, 37003–37026. https://doi.org/10.1039/C4RA06658H
5. Zhang, J., Zhou, P., Liu, J., Yu, J., 2014. New understanding of the difference of photocatalytic activity among anatase, rutile and brookite tiO2. *Physical Chemistry Chemical Physics*, **16**, 20382-6. https://doi.org/10.1039/c4cp02201g
6. Zhang, Q., Duan, J., Zhu, Z., Rong, L., Lin, X., Dong, H., Liu, D., 2024. Tuning oxygen vacancies via photoinduced defect engineering in plasma pre-treated tiO2 for efficient solar-light-driven oxidation of trace methane. *Chemical Engineering Journal*, **497**, 154681. https://doi.org/10.1016/j.cej.2024.154681
7. Khan, S., Cho, H., Kim, D., Han, S.S., Lee, K.H., Cho, S.-H., Song, T., Choi, H., 2017. Defect engineering toward strong photocatalysis of nb-doped anatase tiO2: Computational predictions and experimental verifications. *Applied Catalysis B: Environmental*, **206**, 520-530. https://doi.org/10.1016/j.apcatb.2017.01.039
8. Rawool, S., Yadav, K., Polshettiwar, V., 2021. Defective tiO2 for photocatalytic CO2 conversion to fuels and chemicals. *Chemical Science*, **12**, 4267-4299. https://doi.org/10.1039/d0sc06451c
9. Poolakkandy, R.R., Menamparambath, M.M., 2020. Soft-template-assisted synthesis: A promising approach for the fabrication of transition metal oxides. *Nanoscale Advances*, **2**, 5015-5045. https://doi.org/10.1039/d0na00599a
10. Chen, Z., Ren, X., Yang, L., Fu, N., An, X., 2023. Self-templating synthesis and photocatalytic activity of hollow TiO2 microspheres prepared by the sol–gel+ solvothermal method. *Applied Surface Science*, **619**, 156731.
11. Sunny, N., Mathew, S., Chandel, N., Saravanan, P., Rajeshkannan, R., Rajasimman, M., Vasseghian, Y., Rajamohan, N., Kumar, S., 2022. Green synthesis of titanium dioxide nanoparticles using plant biomass and their applications- A review. *Chemosphere*, **300**, 134612. https://doi.org/10.1016/j.chemosphere.2022.134612
12. Yan, Z., He, J., Guo, L., Li, Y., Duan, D., Chen, Y., Li, J., Yuan, F., Wang, J., 2017. Biotemplated mesoporous tiO2/SiO2 composite derived from aquatic plant leaves for efficient dye degradation. *Catalysts*, **7**, 82. https://doi.org/10.3390/catal7030082
13. Akram, B., Ahmad, K., Khan, J., Khan, B.A., Akhtar, J., 2018. Low-temperature solution-phase route to sub-10 nm titanium oxide nanocrystals having super-enhanced photoreactivity. *New Journal of Chemistry*, **42**, 10947-10952. https://doi.org/10.1039/c8nj02317d
14. Casino, S., Di Lupo, F., Francia, C., Tuel, A., Bodoardo, S., Gerbaldi, C., 2014. Surfactant-assisted sol gel preparation of high-surface area mesoporous tiO2 nanocrystalline li-ion battery anodes. *Journal of Alloys and Compounds*, **594**, 114-121. https://doi.org/10.1016/j.jallcom.2014.01.111
15. Drissi, F., Lahfa, F., Gonzalez, T., Peiretti, F., Tanti, J., Haddad, M., Fabre, N., Govers, R., 2021. A citrullus colocynthis fruit extract acutely enhances insulin-induced GLUT4 translocation and glucose uptake in adipocytes by increasing PKB phosphorylation. *Journal of Ethnopharmacology*, **270**, 113772. https://doi.org/10.1016/j.jep.2020.113772
16. Ouf, S.A., Ali, M.I., Haggag, M.G., Elsafty, D.O., Faraag, A.H.I., 2022. Enhancement of antidermatophytic activities of citrullus colocynthis schrad collected from different ecological habitats in Egypt using fluconazole. *Phytomedicine Plus*, **2**, 100178. https://doi.org/10.1016/j.phyplu.2021.100178
17. Jemai, R., Drira, R., Makni, M., Fetoui, H., Sakamoto, K., 2020. Colocynth (Citrullus colocynthis) seed extracts attenuate adipogenesis by down-regulating PPARγ/SREBP-1c and c/EBPα in 3T3-L1 cells. *Food Bioscience*, **33**, 100491. https://doi.org/10.1016/j.fbio.2019.100491

18. Khan, U.N., Inayat, A., Shah, G.M., Hassan, H.M.A., Zaki, M.E.A., Alanazi, A.A., El-Zahhar, A.A., Noureen, S., Abbas, S.M., 2022. Green synthesis of magnesium oxide nanosheets by using citrullus colocynthis fruit extract and its use in biofuel production. *Biomass and Bioenergy*, **167**, 106640. https://doi.org/10.1016/j.biombioe.2022.106640
19. Talebi Tadi, A., Farhadiannezhad, M., Nezamtaheri, M., Goliaei, B., Nowrouzi, A., 2024. Biosynthesis and characterization of gold nanoparticles from citrullus colocynthis (L.) schrad pulp ethanolic extract: Their cytotoxic, genotoxic, apoptotic, and antioxidant activities. *Heliyon*, **10**, e35825. https://doi.org/10.1016/j.heliyon.2024.e35825
20. Ouerghi, O., Geesi, M.H., Riadi, Y., Ibnouf, E.O., 2022. Limon-citrus extract as a capping/reducing agent for the synthesis of titanium dioxide nanoparticles: Characterization and antibacterial activity. *Green Chemistry Letters and Reviews*, **15**, 483-490. https://doi.org/10.1080/17518253.2022.2094205
21. Ouerghi, O., Geesi, M.H., Riadi, Y., Ibnouf, E.O., Kaiba, A., 2023. Phytosynthesis of anatase tiO2 nanostructures using grapefruit extract for antimicrobial and catalytic applications. *Journal of Sol-Gel Science and Technology*, **108**, 538-547. https://doi.org/10.1007/s10971-023-06215-6
22. Xie, C., Yang, S., Li, B., Wang, H., Shi, J.-W., Li, G., Niu, C., 2016. C-doped mesoporous anatase tiO 2 comprising 10 nm crystallites. *Journal of Colloid and Interface Science*, **476**, 1-8. https://doi.org/10.1016/j.jcis.2016.01.080
23. Byrne, C., Fagan, R., Hinder, S., McCormack, D.E., Pillai, S.C., 2016. New approach of modifying the anatase to rutile transition temperature in TiO 2 photocatalysts. *RSC advances*, **6**, 95232–8.
24. Maras, E., Saito, M., Inoue, K., Jónsson, H., Ikuhara, Y., McKenna, K.P., 2019. Determination of the structure and properties of an edge dislocation in rutile tiO2. *Acta Materialia*, **163**, 199-207. https://doi.org/10.1016/j.actamat.2018.10.015
25. Ren, P., Song, M., Lee, J., Zheng, J., Lu, Z., Engelhard, M., Yang, X., Li, X., Kisailus, D., Li, D., 2019. Edge dislocations induce improved photocatalytic efficiency of colored tiO_2. *Advanced Materials Interfaces*, **6**, 1901121. https://doi.org/10.1002/admi.201901121
26. Huseynov, E.M., Huseynova, E.A., 2023. Infrared spectroscopy of nanocrystalline anatase (TiO2) particles under the neutron irradiation. *Optical Materials*, **144**, 114351. https://doi.org/10.1016/j.optmat.2023.114351
27. Li, Z., Luo, L., Li, M., Chen, W., Liu, Y., Yang, J., Xu, S.-M., Zhou, H., Ma, L., Xu, M., 2021. Photoelectrocatalytic C–H halogenation over an oxygen vacancy-rich TiO2 photoanode. *Nature Communications* 12, 6698.
28. Qian, C., Liu, H., Li, H., Wang, T., Wang, S., 2024. Mesoporous tiO2 spheres with rich oxygen vacancies for enhanced photocatalytic hydrogen production. *International Journal of Hydrogen Energy*, **51**, 605-614. https://doi.org/10.1016/j.ijhydene.2023.08.278
29. Wang, Y., Chen, Y.-X., Barakat, T., Wang, T.-M., Krief, A., Zeng, Y.-J., Laboureur, M., Fusaro, L., Liao, H.-G., Su, B.-L., 2021. Synergistic effects of carbon doping and coating of tiO2 with exceptional photocurrent enhancement for high performance H2 production from water splitting. *Journal of Energy Chemistry*, **56**, 141-151. https://doi.org/10.1016/j.jechem.2020.08.002
30. Qian, C., Liu, H., Li, H., Wang, T., Wang, S., 2024. Mesoporous TiO2 spheres with rich oxygen vacancies for enhanced photocatalytic hydrogen production, International *Journal of Hydrogen Energy* 51, 605–614. https://www.sciencedirect.com/science/article/pii/S0360319923044725 (accessed November 21, 2024).
31. Noorimotlagh, Z., Kazeminezhad, I., Jaafarzadeh, N., Ahmadi, M., Ramezani, Z., Silva Martinez, S., 2018. The visible-light photodegradation of nonylphenol in the presence of carbon-doped tiO2 with rutile/anatase ratio coated on GAC: Effect of parameters and degradation mechanism. *Journal of Hazardous Materials*, **350**, 108-120. https://doi.org/10.1016/j.jhazmat.2018.02.022
32. Liu, S., Yuan, S., Zhang, Q., Xu, B., Wang, C., Zhang, M., Ohno, T., 2018. Fabrication and characterization of black tiO2 with different Ti3+ concentrations under atmospheric conditions. *Journal of Catalysis*, **366**, 282-8. https://doi.org/10.1016/j.jcat.2018.07.018
33. Nikolay, T., Larina, L., Shevaleevskiy, O., Ahn, B.T., 2011. Electronic structure study of lightly nb-doped tiO2 electrode for dye-sensitized solar cells. *Energy & Environmental Science*, **4**, 1480. https://doi.org/10.1039/c0ee00678e
34. Sanjinés, R., Tang, H., Berger, H., Gozzo, F., Margaritondo, G., Lévy, F., 1994. Electronic structure of anatase tiO2 oxide. *Journal of Applied Physics*, **75**, 2945-2951. https://doi.org/10.1063/1.356190
35. Gu, Z., Cui, Z., Wang, Z., Sinkou Qin, K., Asakura, Y., Hasegawa, T., Hongo, K., Maezono, R., Yin, S., 2021. Intrinsic carbon-doping induced synthesis of oxygen vacancies-mediated tiO2 nanocrystals: Enhanced photocatalytic NO removal performance and mechanism. *Journal of Catalysis*, **393**, 179-189. https://doi.org/10.1016/j.jcat.2020.11.025
36. Negi, C., Kandwal, P., Rawat, J., Sharma, M., Sharma, H., Dalapati, G., Dwivedi, C., 2021. Carbon-doped titanium dioxide nanoparticles for visible light driven photocatalytic activity. *Applied Surface Science*, **554**, 149553. https://doi.org/10.1016/j.apsusc.2021.149553
37. Di Valentin, C., Pacchioni, G., Selloni, A., 2005. Theory of carbon doping of titanium dioxide. *Chemistry of Materials*, **17**, 6656-6665. https://doi.org/10.1021/cm051921h
38. Gautam, S., Agrawal, H., Thakur, M., Akbari, A., Sharda, H., Kaur, R., Amini, M., 2020. Metal oxides and metal organic frameworks for the photocatalytic degradation: A review. *Journal of Environmental Chemical Engineering*, **8**, 103726. https://doi.org/10.1016/j.jece.2020.103726
39. Kaykhaii, M., Hashemi, S.H., Andarz, F., Piri, A., Sargazi, G., 2021. Chromium-based metal organic framework for pipette tip micro-solid phase extraction: an effective approach for determination of methyl and propyl parabens in wastewater and shampoo samples. *BMC Chemistry*, **15**, 60. https://doi.org/10.1186/s13065-021-00786-7
40. Kaykhaii, M., Yavari, E., Sargazi, G., Ebrahimi, A.K., 2020. Highly sensitive determination of Bisphenol A in bottled water samples by HPLC after its extraction by a novel th-MOF pipette-tip micro-SPE. *Journal of Chromatographic Science*, **58**, 373-382. https://doi.org/10.1093/chromsci/bmz111
41. Cui, W., Luo, S., Hou, H., Wu, Z., An, B., Xu, M., Ma, C., Liu, S., Li, W., 2024. The synthesis of tiO2 using a nanocrystalline cellulose template improves its photocatalytic performance. *Ceramics International*, **50**, 52218-52227. https://doi.org/10.1016/j.ceramint.2024.09.327